RX210

Motor Control with Space Vector Modulation

R01AN1193ET0101
Rev.1.01
Jan 23, 2013

Introduction

The objective of this project is to implement RX210 MCU base application board and software control reference for Permanent Magnetic Synchronous Motor (PMSM) control with Power Factor Corrector (PFC).

Target Device

RX210

Contents

1. Specifications

- Target Device: RX210

  PFC
  - Input voltage: 110 V AC/60 Hz
  - Output voltage: 200V DC
  - Output power: 400W
  - Power factor: >0.9
  - Current Control Mode: Average current mode
  - Controller Type: PI Controller
  - Carrier Frequency: 20 kHz
  - Module: One phase Time

  PFC
  - Power: 300 W
  - Rated speed: 3000 rpm
  - Type: Surface mount PMSM
  - Module: Three phase Timer
  - Controller: Speed and current control
  - Controller Type: PI Controller
  - Carrier Frequency: 20 kHz

Figure 1 and Figure 2 shows the block diagram for the implementation of PFC and PMSM drives. As shown in Figure 1, RX210 is used to realize the control software of PFC and PMSM drives. In Figure 1, average current mode and speed/current control are realized in software using RX210. Table 1 and Table 2 show the specifications of PFC and PMSM used in this project.

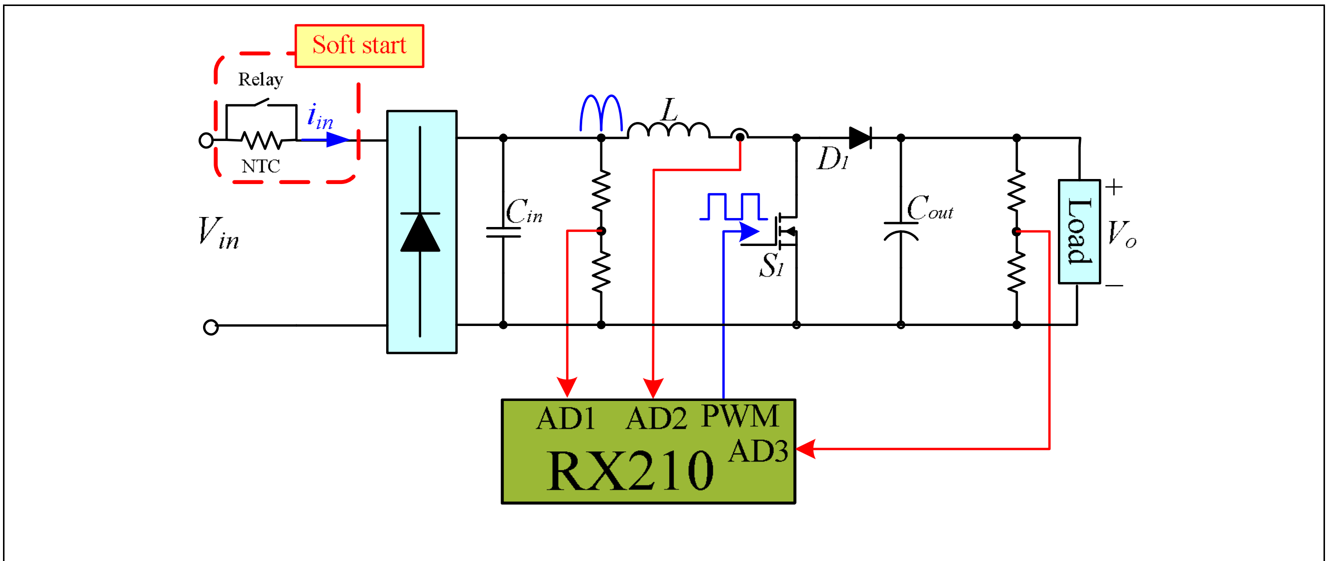

Figure 1 Power Factor Corrector

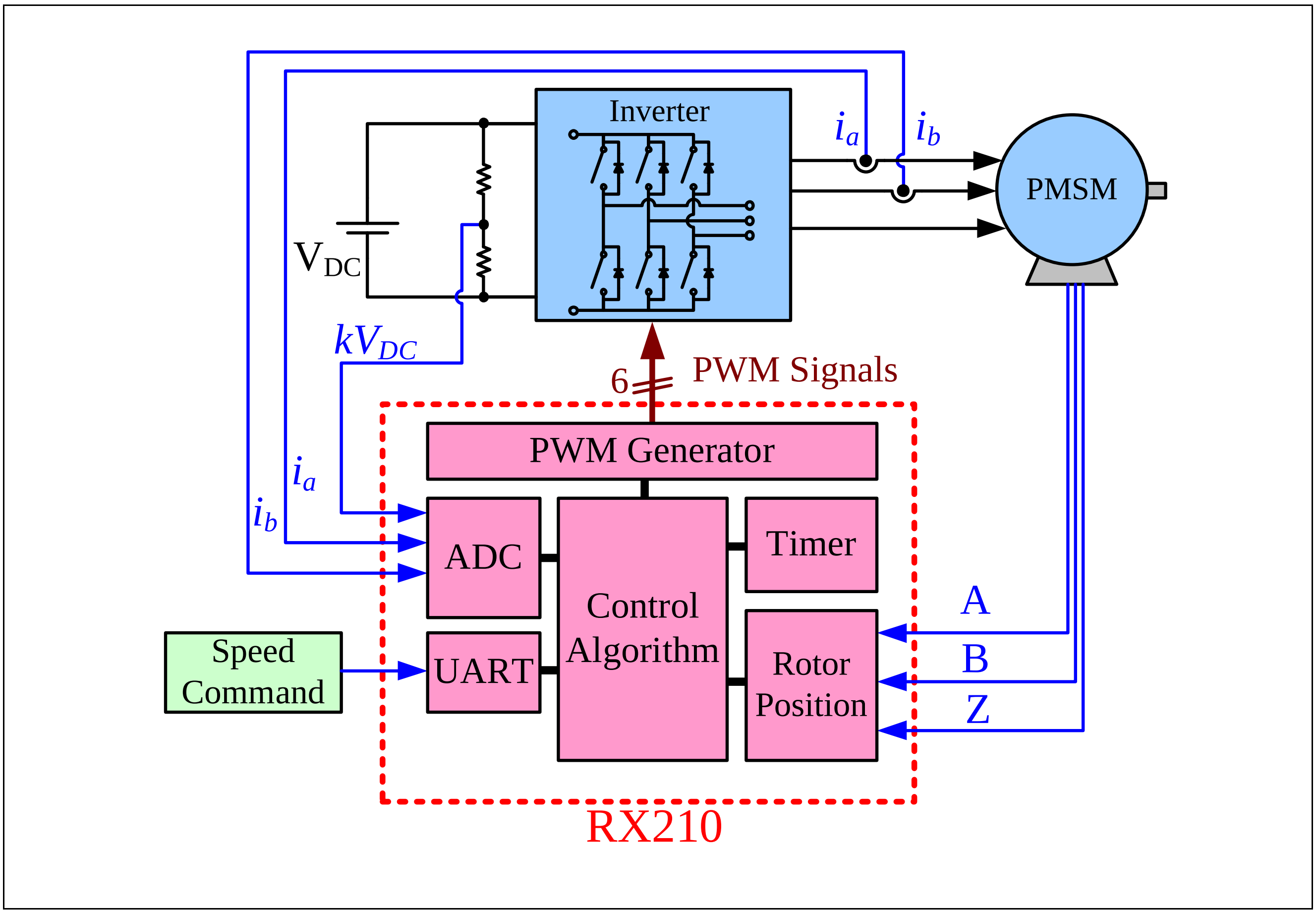

Figure 2 Vector-controlled PMSM drive

Table 1 Specifications of PFC

Parameters	Value
Input voltage, V_{in}	• 110VAC/60Hz
Output voltage, V_{out}	• 220VDC
Power rate, P_o	• 400W
Current control mode	• Average current mode control
Power factor	• 0.90-0.98
Switching frequency	• 20KHz

Table 2 Specifications of PMSM

Parameters	Value
Rated Power	• 300W
Rated Current (rms)	• 2A
Rated Speed	• 3000 RPM
Rated Torque	• 0.95 Nt-m
Poles No.	• 8
Encoder Resolution	• 2000 C/T
q-axis Stator Inductance (Lqs)	• 5.63 mH
d-axis Stator Inductance (Lds)	• 6.47 mH
Flux Linkage (λ_m)	• 0.06 V-s/rad
Stator Resistance (Rs)	• 2.65Ω

2. PFC Controller Design

Table 3 shows the circuit parameters of the designed PFC. The block diagram of the implementation is shown in Figure 3. As shown in Figure 3, the output voltage is sensed to give the magnitude of current reference via the voltage controller. Furthermore, the input voltage is fed back to give the waveform of the reference current. The input current is sensed and compared with its reference value to generate the duty via current controller. The design specifications of controllers are as follows:

1. Controller Design of current loop
   A. Bandwidth of current loop < 2k Hz
   B. Phase margin > 45 degrees

2. Controller Design of voltage loop
   A. Bandwidth of voltage loop < 120 Hz
   B. Phase margin > 45 degrees

Table 3 Circuit parameters of PFC

Parameters	Value
Input voltage (V_{in})	• 110 V rms
Output voltage (V_o)	• 200 VDC
Input current (I_L)	• 3.63A rms
Inductor (L)	• 1321.7 μH
Capacitor (C)	• 943 μF
Inductor DCR (R_{DCR})	• 125.3 mΩ
Capacitor ESR (R_{ESR})	• 76.37 mΩ
MOSFET on-resistance (R_{on})	• 0.175 Ω
Output power (P_o)	• 400 W
Switching frequency (f_{sw})	• 20 KHz

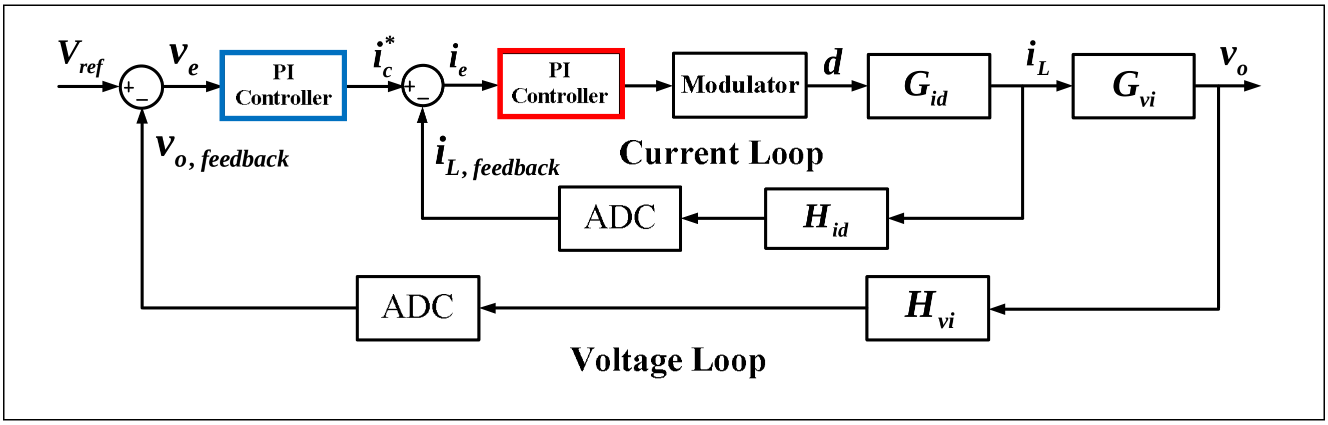

Figure 3 Block diagram of the developed PFC

2.1 Controller Design of Current Loop

The Bode plot for current loop is shown in Figure 4. As shown in Figure 4, the current loop band width BW= 1.18 kHz and PM = 70.4°. The designed results are:

$$PI\ \ controller = 0.2319 + \frac{634.09375}{s}$$

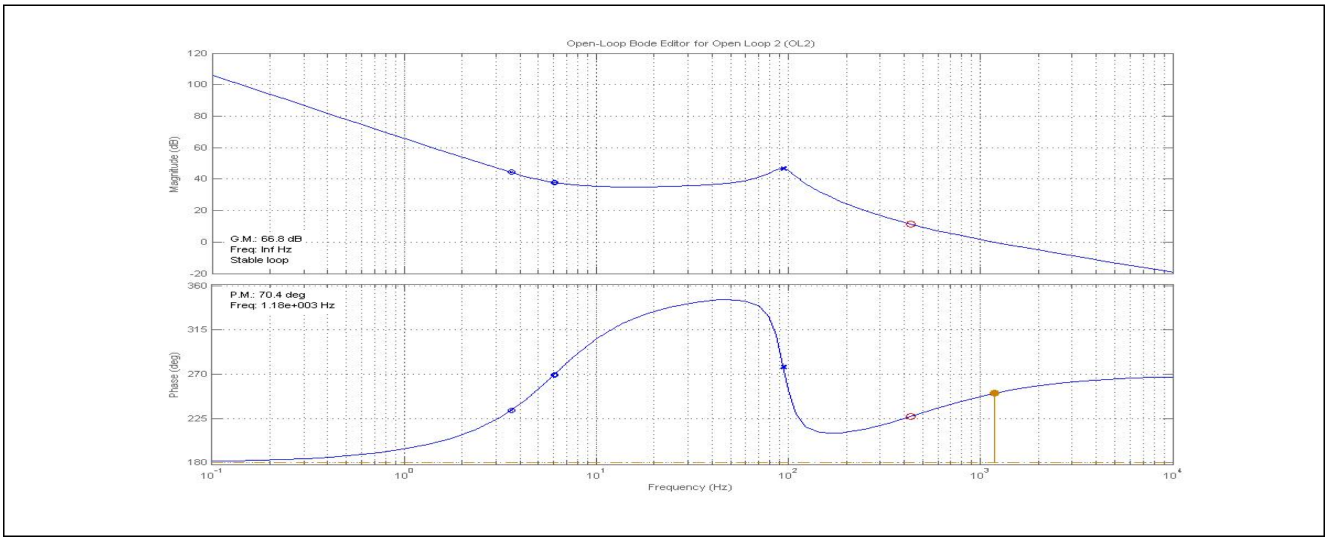

Figure 4 Bode lot of current loop

2.2 Controller Design of voltage loop

Figure 5 shows the Bode plot of voltage loop and the bandwidth of voltage loop is BW = 6.54Hz, PM = 70.8°. The designed results are:

$$PI\ \ controller = 1.7119 + \frac{77.84375}{s}$$

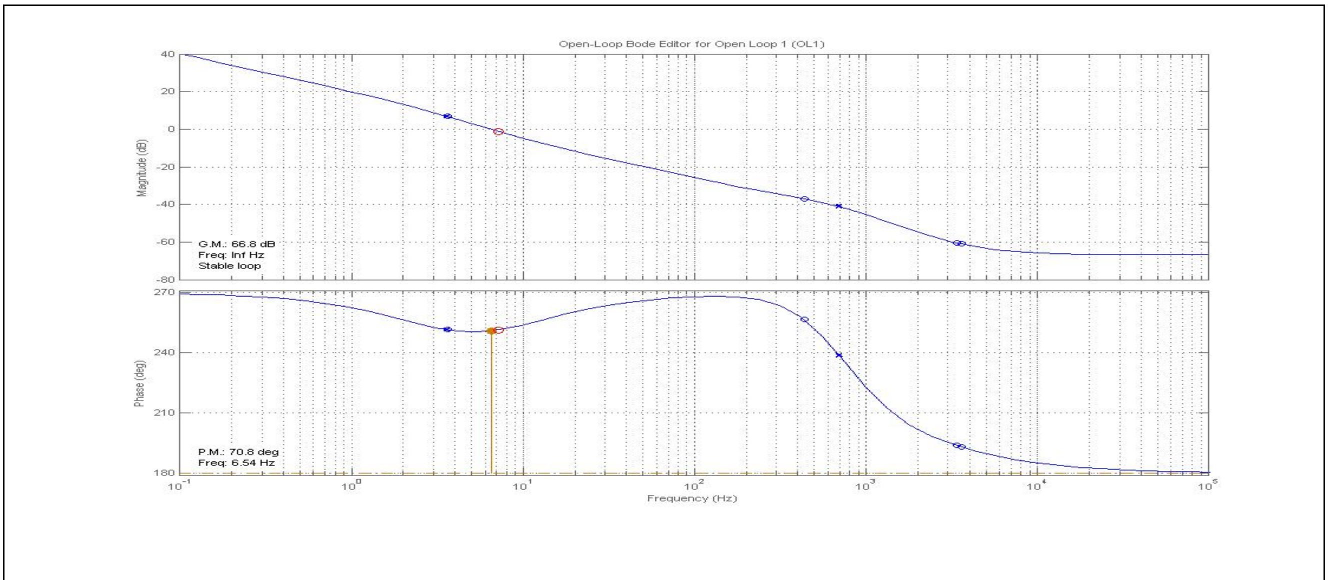

Figure 5 Bode lot of voltage loop

3. Controller Design of PMSM Drives

3.1 Modeling of PMSM

The mathematical model of PMSM referring to the synchronous reference frame can be derived as follows.

Voltage equations:

$$\begin{bmatrix} v_{ds}^e \\ v_{qs}^e \end{bmatrix} = \begin{bmatrix} R_s + L_d p & -\omega_e L_q \\ \omega_e L_d & R_s + L_q p \end{bmatrix} \begin{bmatrix} i_{ds}^e \\ i_{qs}^e \end{bmatrix} + \begin{bmatrix} 0 \\ \omega_e i_{fd} L_{md} \end{bmatrix} \tag{1}$$

Torque equation:

$$T_e = \frac{3}{2} \cdot \frac{P}{2} \left[\lambda_{ds}^e i_{qs}^e - \lambda_{qs}^e i_{ds}^e \right] \tag{2}$$

Flux equations:

$$\lambda_{ds}^e = L_d i_{ds}^e + L_{md} i_{fd} \tag{3}$$

$$\lambda_{qs}^e = L_q i_{qs}^e \tag{4}$$

The state equation for the electrical circuit can be revised from (1) and shown in (5).

$$p \begin{bmatrix} i_{ds}^e \\ i_{qs}^e \end{bmatrix} = \begin{bmatrix} -\dfrac{R_s}{L_d} & 0 \\ 0 & -\dfrac{R_s}{L_q} \end{bmatrix} \begin{bmatrix} i_{ds}^e \\ i_{qs}^e \end{bmatrix} + \begin{bmatrix} \dfrac{1}{L_d}(v_{ds}^e + \omega_e L_q i_{qs}^e) \\ \dfrac{1}{L_q}(v_{qs}^e - \omega_e L_d i_{ds}^e - \omega_e L_{md} i_{fd}) \end{bmatrix} \tag{5}$$

As shown in (2), the torque can be controlled via q-axis current regulation if the controller keeps the d-axis current component equal to zero. By (2), (3), and (4), the torque equation becomes:

$$T_e = \frac{3}{2} \cdot \frac{P}{2} \left[\left(L_d - L_q \right) i_{ds}^e i_{qs}^e + \lambda_m i_{qs}^e \right] \tag{6}$$

When the d-axis current component of magnetizing current equals to zero, the torque equation can be rewritten as:

$$T_e = \frac{3}{2} \cdot \frac{P}{2} (L_{md} i_{fd} i_{qs}^e) = \frac{3}{2} \cdot \frac{P}{2} (\lambda_m i_{qs}^e) \tag{7}$$

Since the flux is constant (no demagnetization) for constant torque operation, the torque is controlled by the q-axis current. Furthermore, since the rotor flux, which aligns along the d-axis of synchronous frame, is perpendicular to the torque producing current, q-axis component of stator current, maximum torque can be obtained.

3.2 Vector Control of PMSM

The block diagram of vector-controlled PMSM drives for speed control/current control is shown in Figure 6. As shown in Figure 6, the PMSM drives consist of three controllers, including speed controller, q-axis and d-axis current controllers. To achieve decoupling control between q-axis and d-axis components, such that the linear control law can be used, the voltage decoupling mechanism is invoked in Figure 6. The decoupling terms shown in (8) and (9) are derived from (5). By (5), the block diagram for current controller design can be derived.

$$\begin{bmatrix} v_{ds}^e \\ v_{qs}^e \end{bmatrix} = L_d \begin{bmatrix} p + \dfrac{R_s}{L_d} & 0 \\ 0 & p + \dfrac{R_s}{L_q} \end{bmatrix} \begin{bmatrix} i_{ds}^e \\ i_{qs}^e \end{bmatrix} + \begin{bmatrix} -\omega_e L_q i_{qs}^e \\ \omega_e L_d i_{ds}^e + \omega_e L_{md} i_{fd}) \end{bmatrix} \tag{8}$$

$$\begin{bmatrix} v_{dsdecouple}^e \\ v_{qsdecouple}^e \end{bmatrix} = \begin{bmatrix} -\omega_e L_q i_{qs}^e \\ \omega_e L_d i_{ds}^e + \omega_e L_{md} i_{fd}) \end{bmatrix} \tag{9}$$

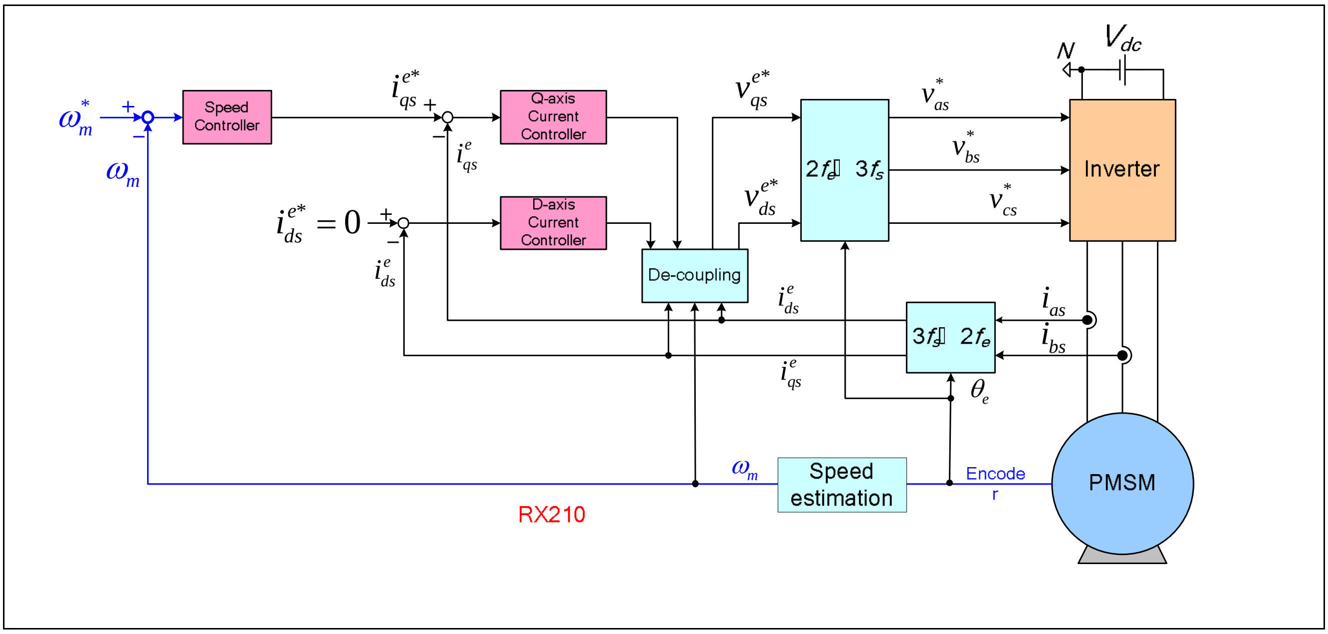

Figure 6 Block diagram of vector-controlled PMSM drives

3.3 Space Vector Modulation

A carried based PWM method which is shown to be equivalent as discussed in [1]. Based upon this method, the maximum linear modulation index can be extended from 1.0 p.u. to 1.1547 p.u.; base voltage = 0.5 Vdc. Moreover, V_{as}^*, V_{bs}^*, V_{cs}^* are used as reference to give T_a^*, T_b^*, *and* T_c^* which are ratios of phase voltage references to the half DC-link voltage, respectively. By these values, the related minimum and maximum are and used to give the pulse shift time as shown in (12). And the new pulse time is modified as shown in (13) to (15) to centralize the pulse in the half switching period as shown in Figure 7 in order to extend the linear modulation index.

$$T_{\max} = \max\left\{T_a^*, T_b^*, T_c^*\right\} \quad (10)$$

$$T_{\min} = \min\left\{T_a^*, T_b^*, T_c^*\right\} \quad (11)$$

$$T_0 = \frac{1}{2}\left(T_s - T_{\max} - T_{\min}\right) \quad (12)$$

$$T_a = T_a^* + T_0 \quad (13)$$

$$T_b = T_b^* + T_0 \quad (14)$$

$$T_c = T_c^* + T_0 \quad (15)$$

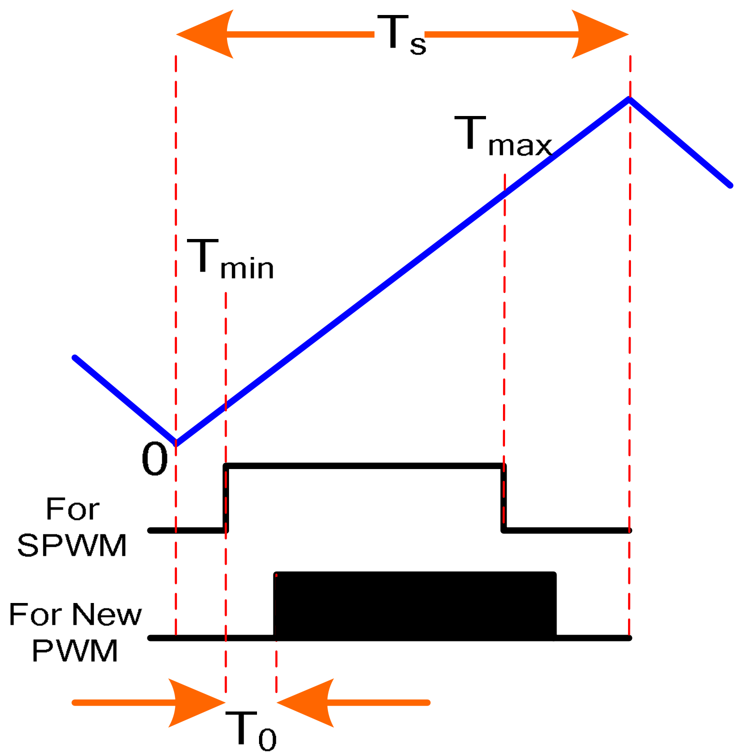

Figure 7 Diagram of T_0 component calculation

3.4 Design of d-axis Current Controller

Figure 8 shows the block diagram for d-axis current controller and its related plant. The designed bandwidth is 2 kHz. For the transfer function shown in (16), the closed-loop transfer function can be derived as shown in (17). Based upon pole-zero cancellation method, the relationship between the controller parameters and the plant parameter can be derived and shown in (18). The closed-loop transfer function with pole-zero cancellation can be further simplified as shown in (19). Therefore, the parameters of controller are derived as shown in (20) provided the bandwidth is given. The Bode plot for d-axis current controller is shown in Figure 9. As shown in Figure 9, the d-axis current controller band width BW = 2 kHz and magnitude = -3.04 dB.

$$G_{id}(s) = \frac{1}{R_s + L_{ds}s} = \frac{1}{2.65 + 6.4775 \times 10^{-3} s} \quad (16)$$

$$T_d(s) \triangleq \frac{i_{ds}^{e}}{i_{ds}^{e*}} = \frac{(\frac{K_p s + K_i}{s})(\frac{1}{R_s + L_{ds}s})}{1 + (\frac{K_p s + K_i}{s})(\frac{1}{R_s + L_{ds}s})} \quad (17)$$

$$Let \ \frac{K_p}{K_i} = \frac{L_{ds}}{R_s} \quad (18)$$

Td(s) can be rewritten as follow:

$$T_d(s) = \frac{K_i / R_s}{s + (K_i / R_s)} \quad (19)$$

$$K_i = 2.65 \times 12.566 \times 10^3 = 33299.9$$

$$K_i = \left(6.4775 \times 10^{-3} / 2.65\right) \times 33299.9 = 81.396265 \quad (20)$$

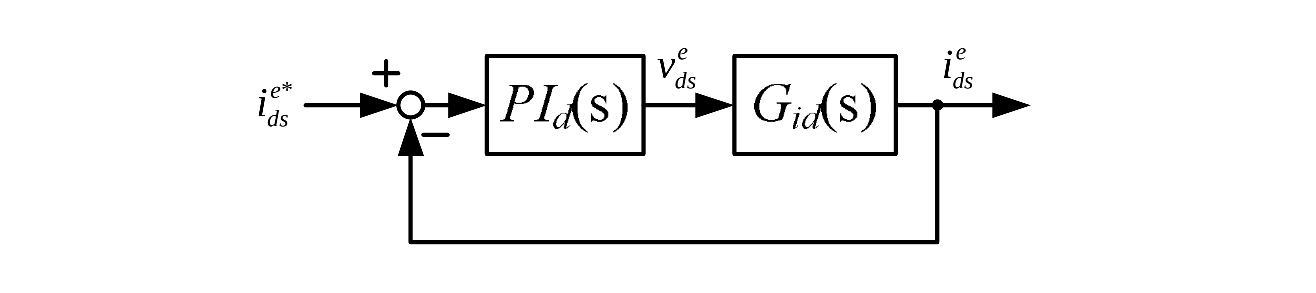

Figure 8 Block diagram for d-axis current controller design

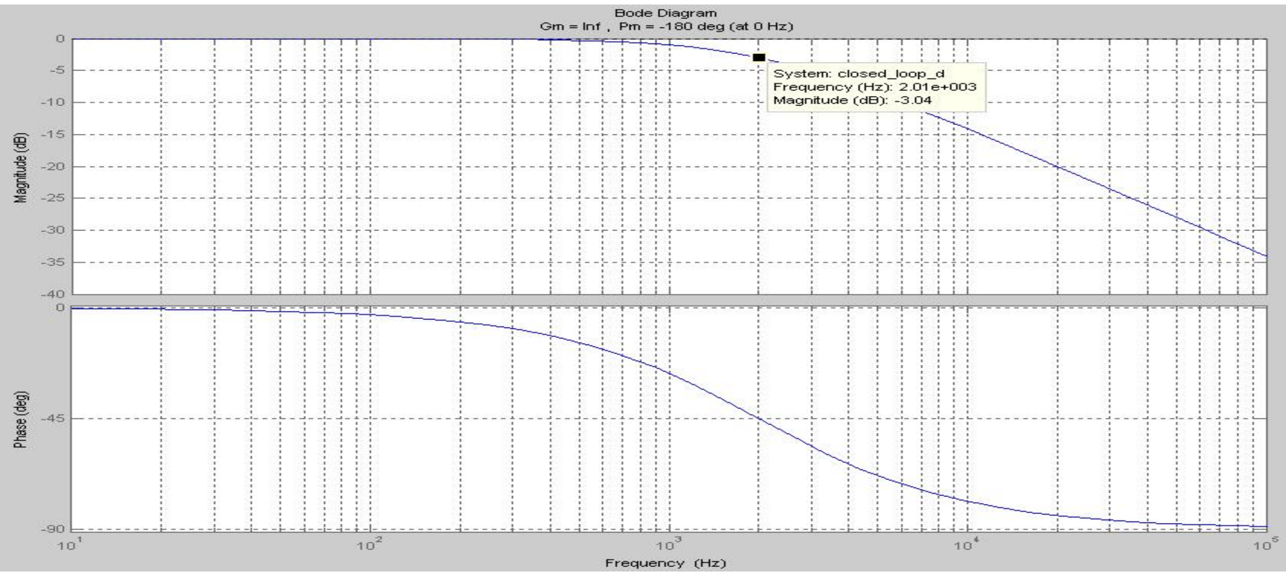

Figure 9 Bode plot of d-axis current controller

3.5 Design of q-axis Current Controller

Figure 10 shows the block diagram for q-axis current controller and its plant. The designed bandwidth is also 2 kHz. Similarly, the parameters of controller are derived as shown in (21) provided the bandwidth is given. The Bode plot for q-axis current controller is shown in Figure 11. As shown in Figure 11 the q-axis current controller band width BW = 2 kHz and magnitude = -3.02 dB.

$$K_i = 2.65 \times 12.566 \times 10^3 = 33299.9$$
$$K_i = \left(5.634 \times 10^{-3} / 2.65\right) \times 33299.9 = 70.796844 \quad (21)$$

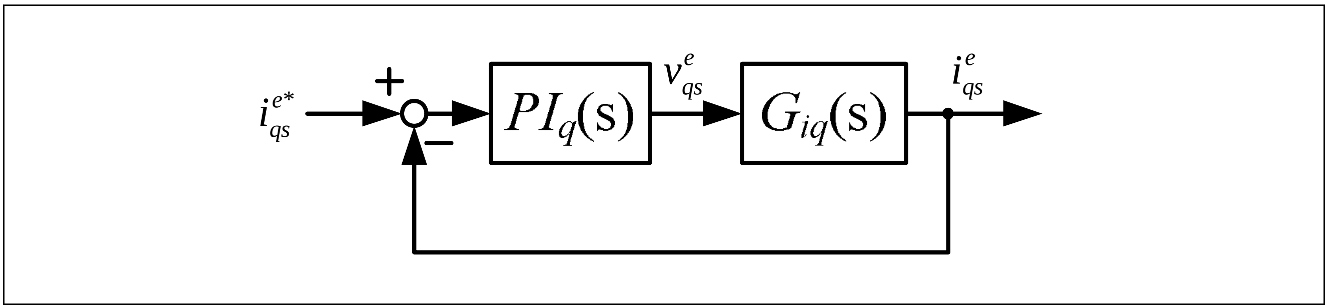

Figure 10 Block diagram for q-axis current controller design

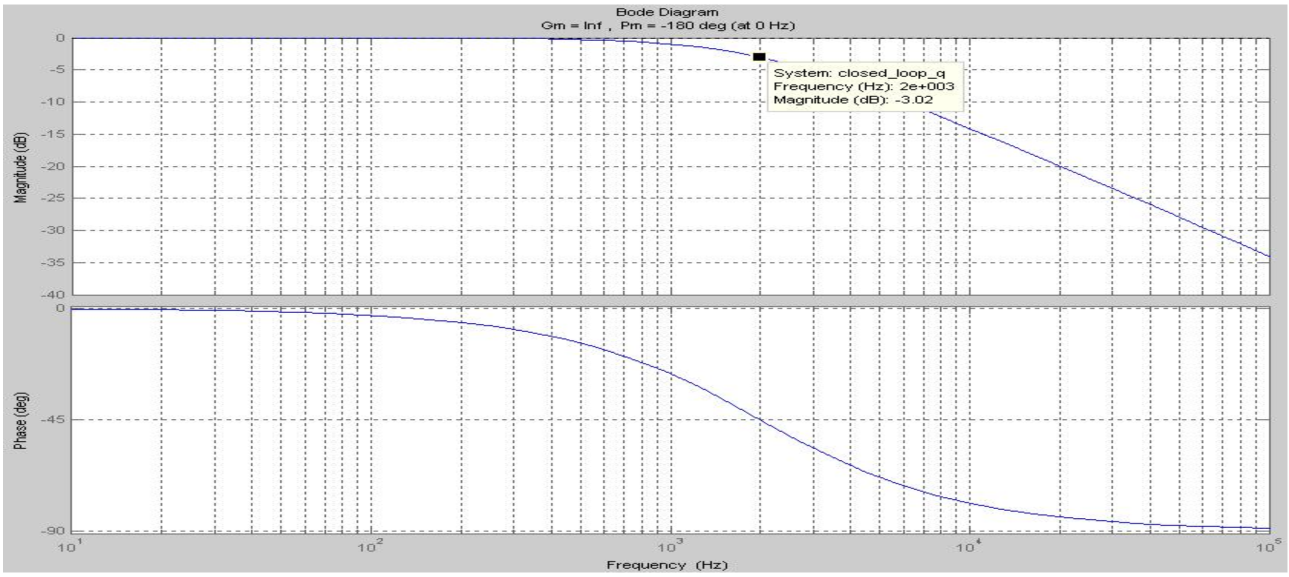

Figure 11 Bode plot of q-axis current controller

3.6 Design of Speed Controller

Figure 12 shows the block diagram for speed controller and its plant. The designed bandwidth is 200 Hz. For the transfer function shown in (22), the closed-loop transfer function can be derived as shown in (23). Based upon pole-zero cancellation method, the relationship between the controller parameters and the plant parameter can be derived and shown in (24). The closed-loop transfer function with pole-zero cancellation can be further simplified as shown in (25). Therefore, the parameters of controller are derived as shown in (26) provided the bandwidth is given. The Bode plot for speed controller is shown in Figure 13. As shown in Figure 13, the speed controller band width BW = 200Hz and magnitude = -3.06 dB.

$$G_t(s) = \frac{\omega_r}{B + J_s} = \frac{1}{0.0033 + 0.0008s} \tag{22}$$

Where

$$J = 0.0008\ kg - m^2$$

$$B = 0.0033\ Nt - m/(rad/\sec)$$

$$T_{speed}(s) = \frac{(K_p + \frac{K_i}{s})(\frac{1}{J_s + B})}{1 + (K_p + \frac{K_i}{s})(\frac{1}{J_s + B})} \tag{23}$$

$$Let\ \frac{K_p}{K_i} = \frac{J}{B} \tag{24}$$

Tspeed(s) can be rewritten as follow:

$$T_{speed}(s) = \frac{K_p / J}{s + K_p / J} \tag{25}$$

$$\because J = 0.0008\ kg - m^2 \quad \therefore K_p = 0.36161$$

$$\because B = 0.0033\ Nt - m^2 \quad \therefore K_i = K_p \frac{B}{J} = 1.49165 \tag{26}$$

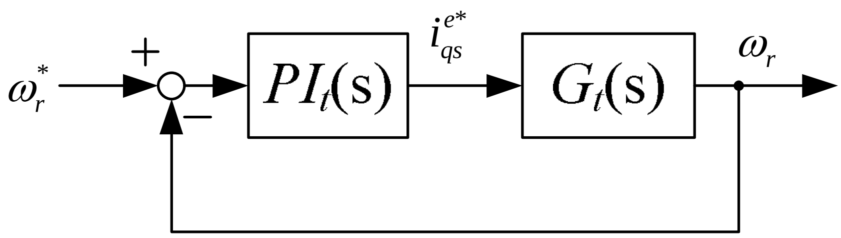

Figure 12 Block diagram for speed controller design

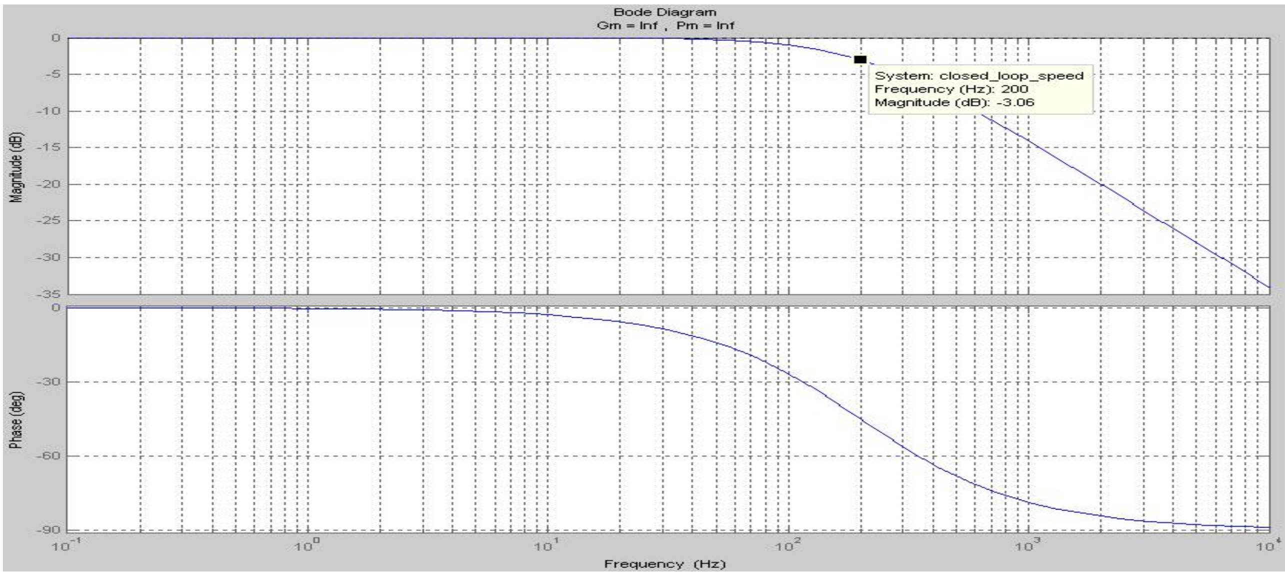

Figure 13 Bode plot of speed controller

4. Start Up Procedure

Figure 14 shows the two phase conduction mode and Figure 15 shows the three phase conduction mode, Figure 16 is the relationship of rotor attracts position from two phase conduction mode and three phase conduction mode, LS series location is two phase conduction mode, and LV series location is three phase conduction mode.

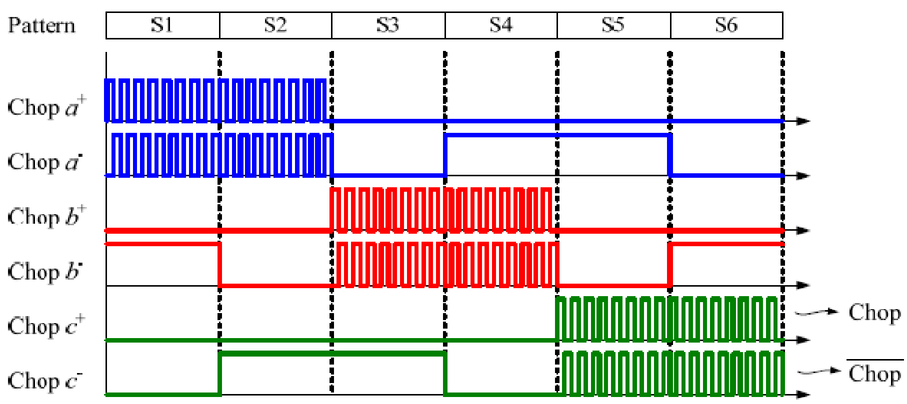

Figure 14 Two phase conduction mode

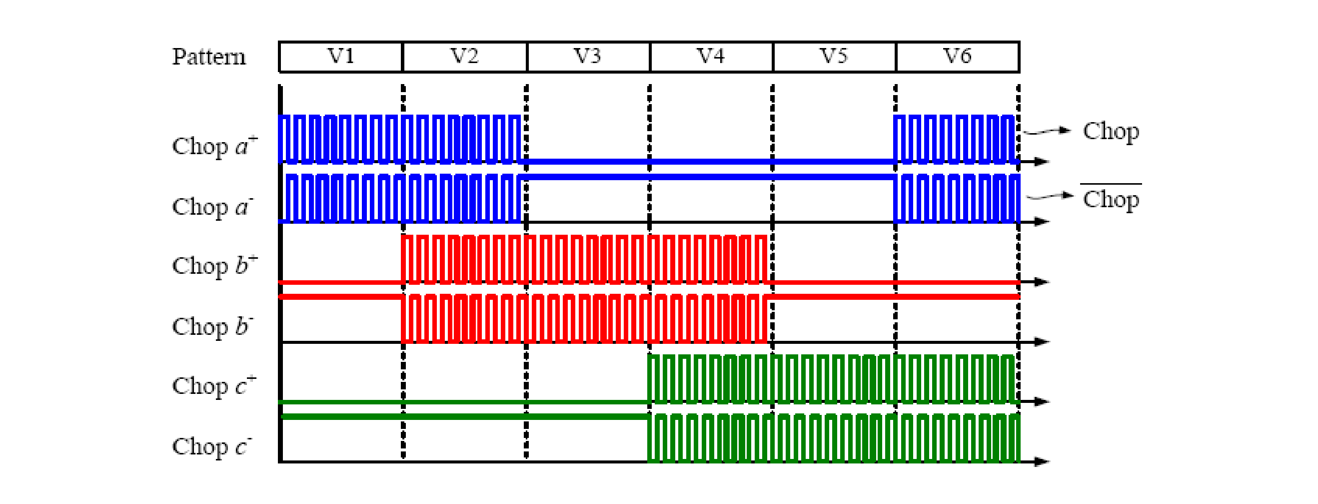

Figure 15 Three phase conduction mode

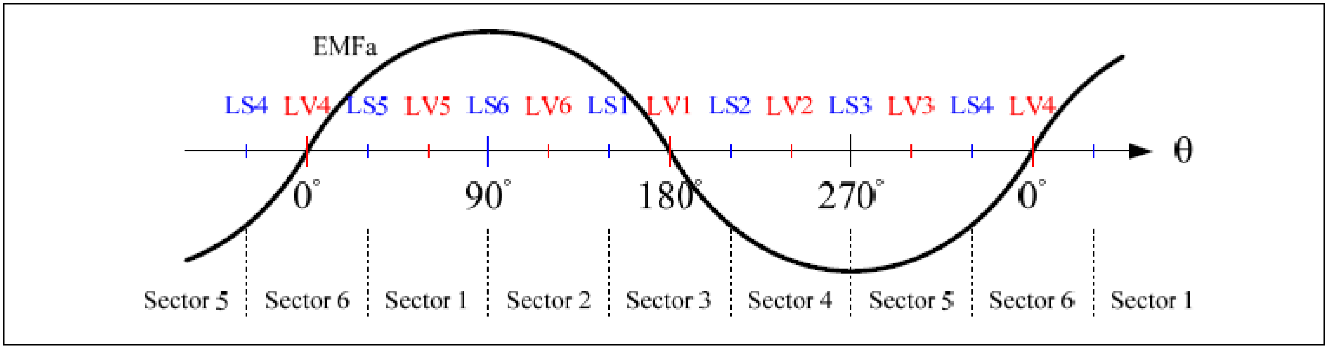

Figure 16 The relationship of rotor position

5. Software Implementation

Figure 17 shows the flow chart of PFC software implementation.

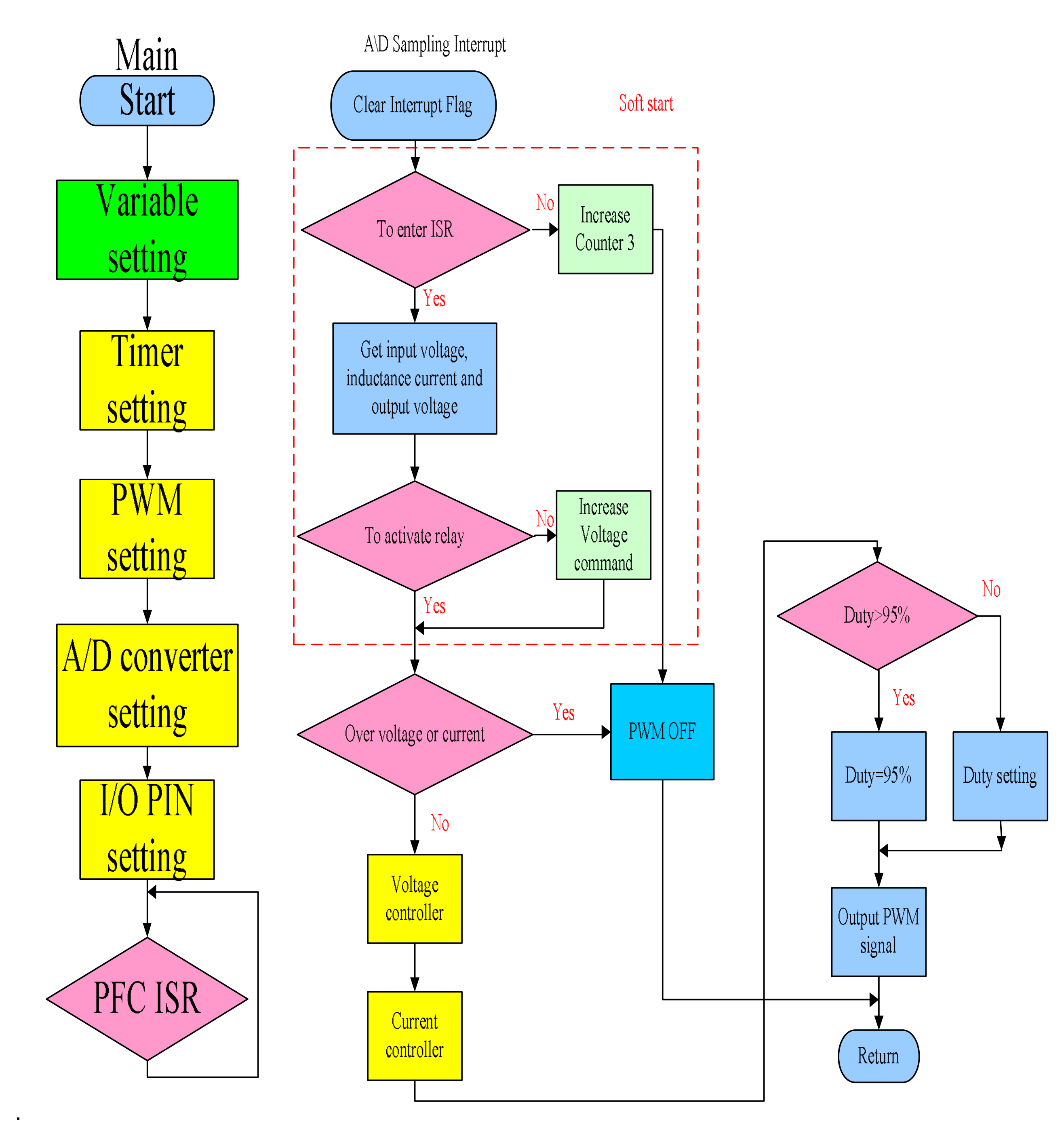

Figure 17 Flow chart of PFC software implementation

Figure 18 shows the flow chart of motor control software implementation.

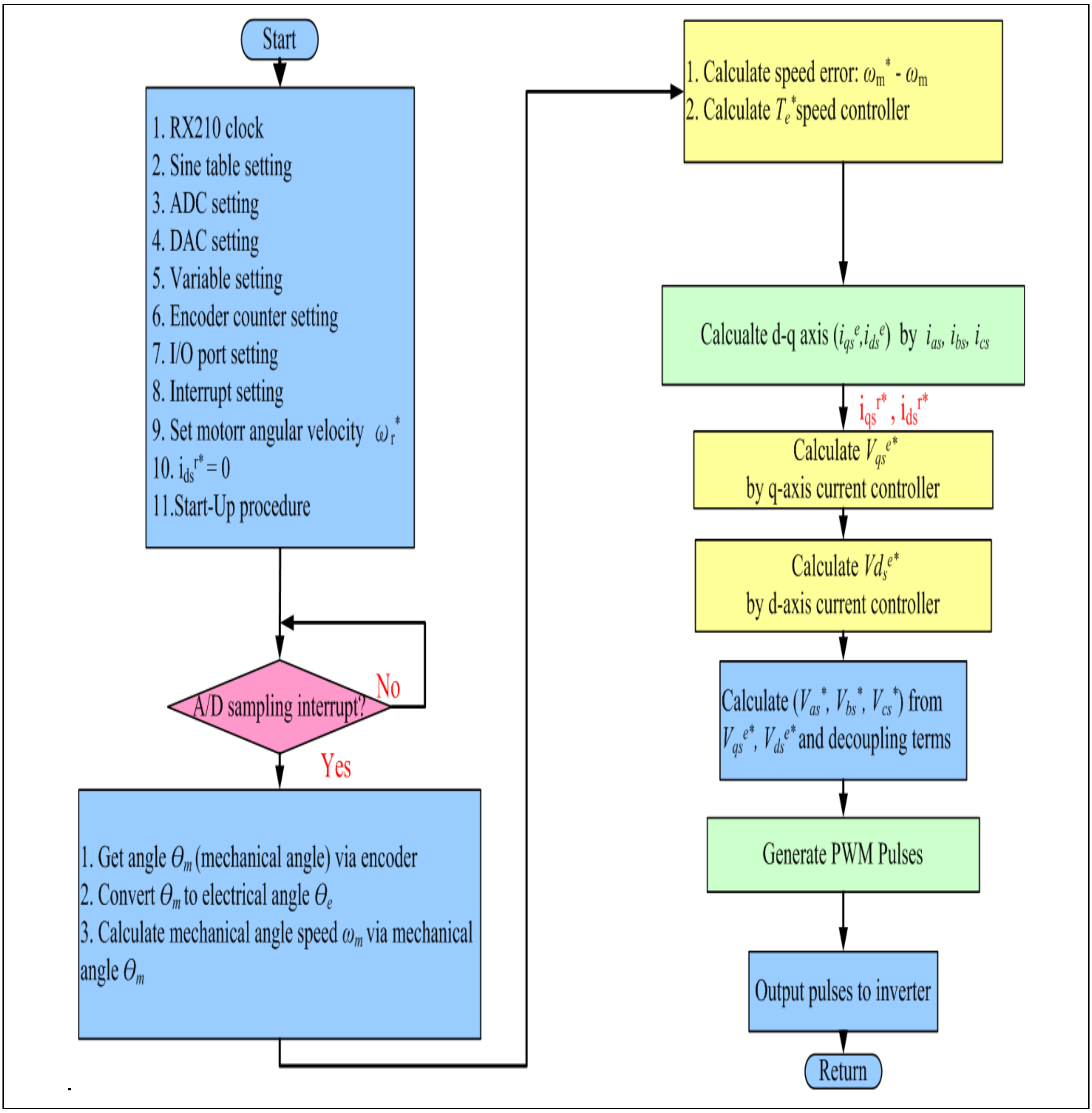

Figure 18 Flow chart of motor control software implementation

6. Experimental Results

Figure 19 shows the experimental set-up. The experimental system for integration test for PFC and vector controlled PMSM drives. The required calculations of block diagram shown in Figure 3 and Figure 6 are realized by RX210-based controlled board as shown in Fig. 20.

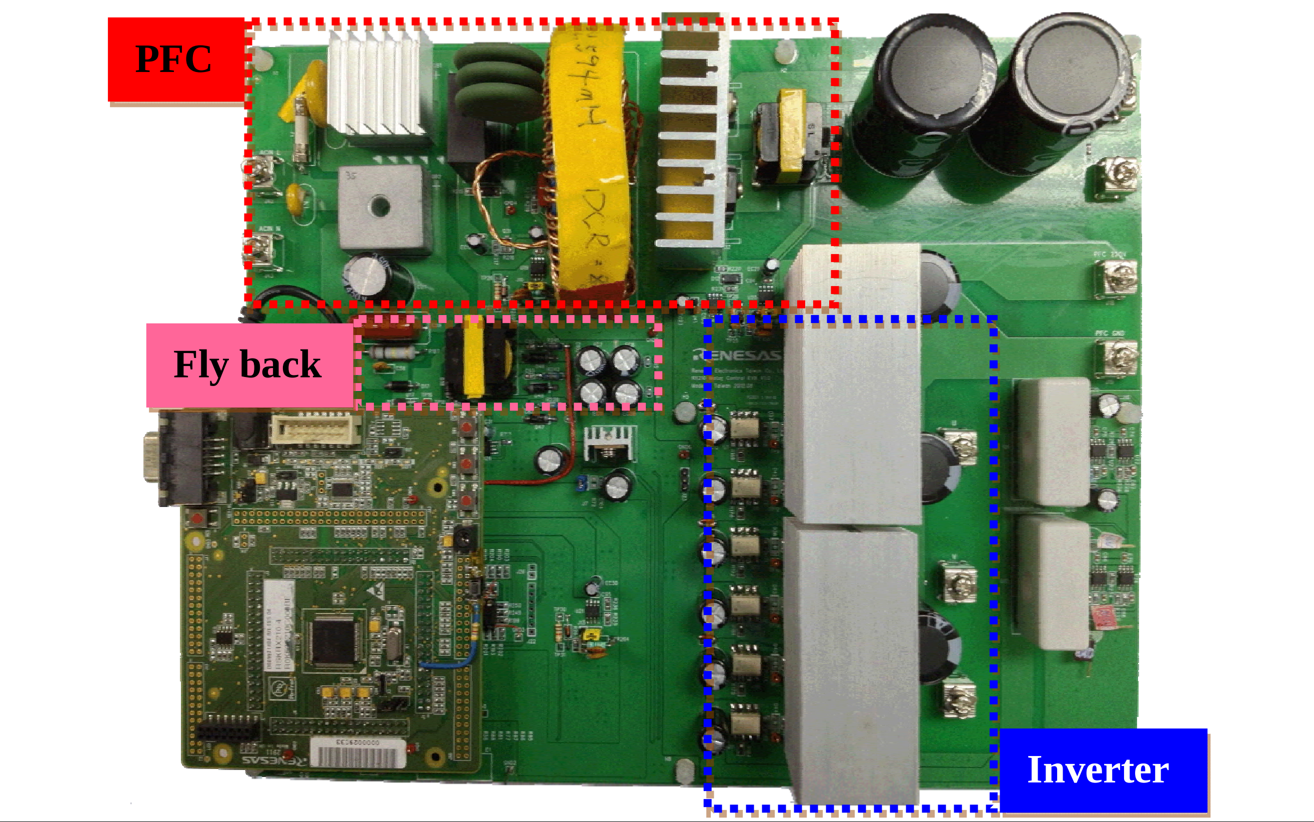

Figure 19 Experimental set up

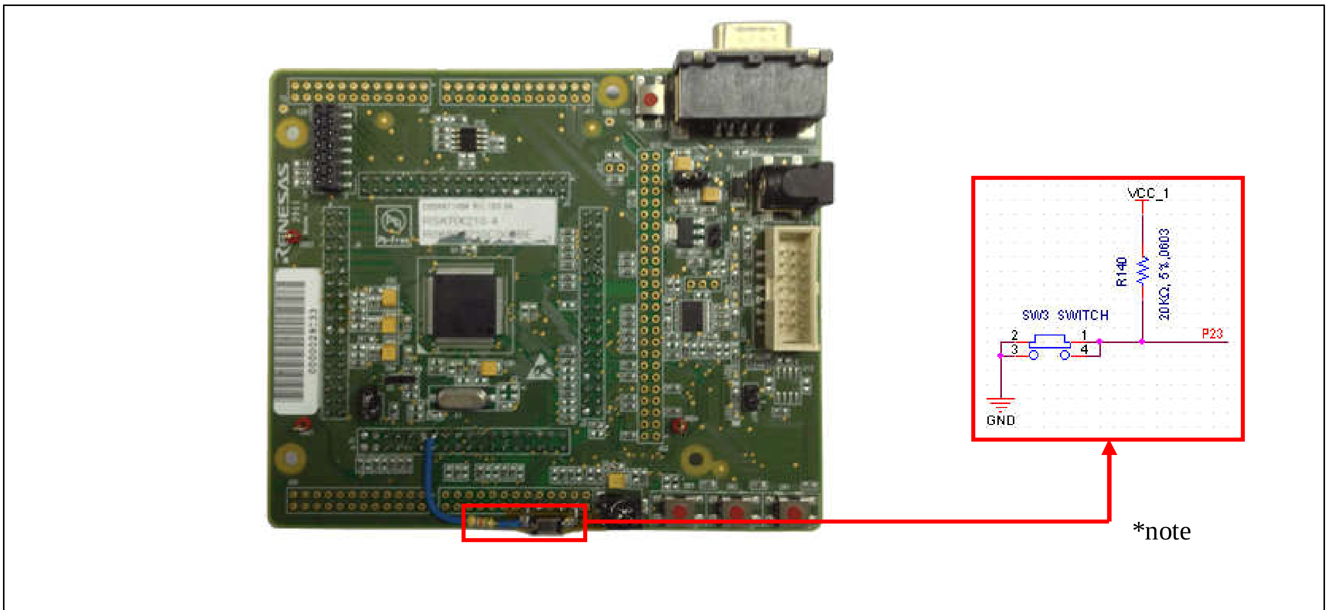

Figure 20 RX210-based control board

Note: A pin is connected with a pull-high resister and a switch button on the RSK, which is used to enable motor control procedure (i.e. P23 = low voltage, motor control start flag == 1)/

Figure 21 and Figure 22 shows the measured waveforms of power factor corrector without motor control. The experimental results show the power factor goes up to 0.98 under full load (400W) condition.

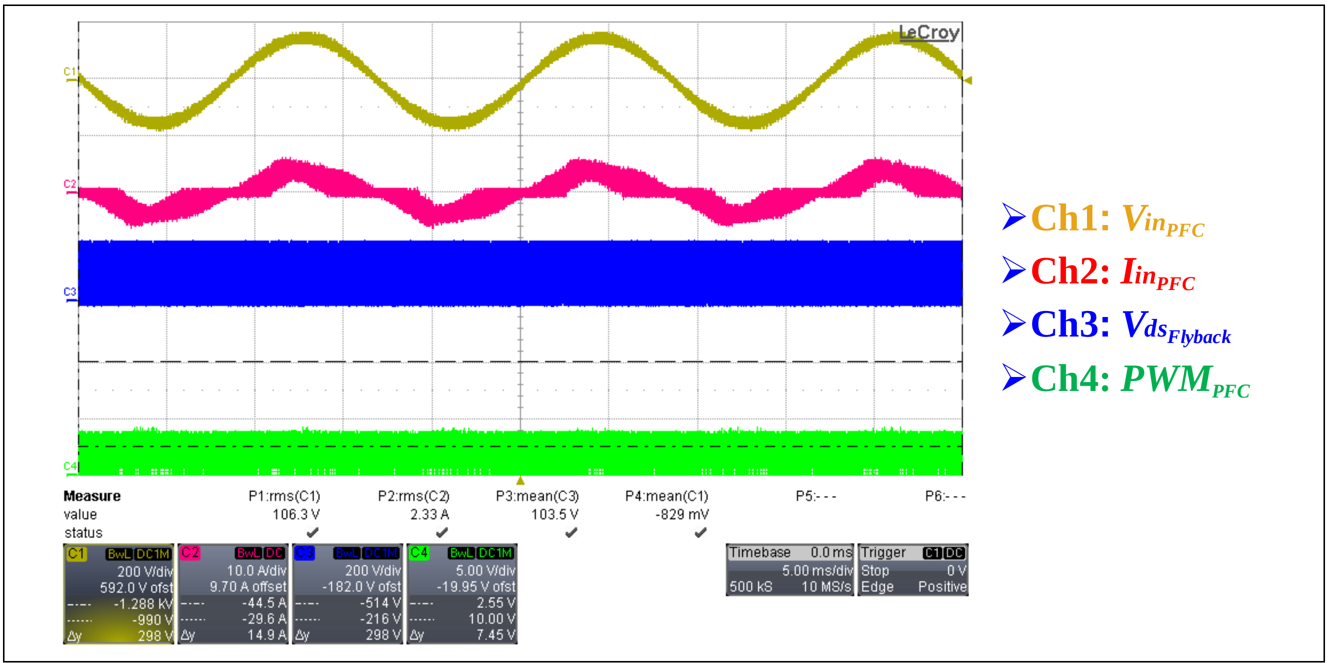

Figure 21 Load = 200W, Vout = 205.5V, PF = 0.963

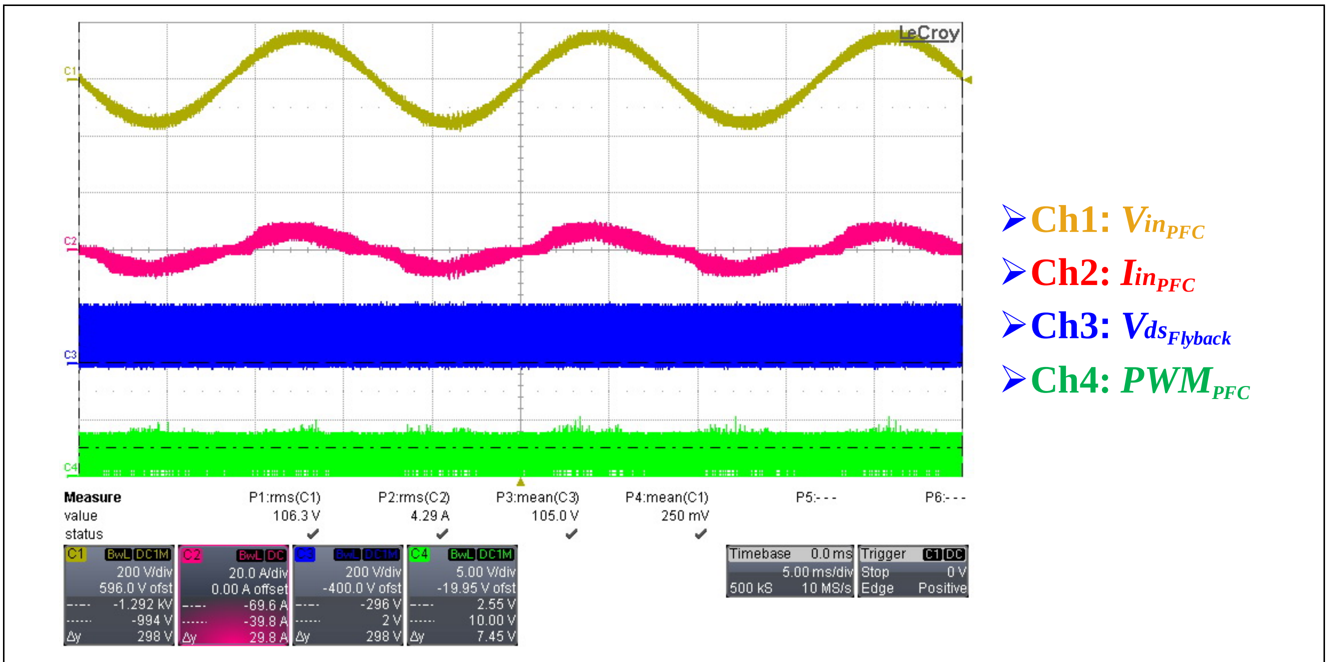

Figure 22 Load = 400W, Vout = 205.5V, PF = 0.982

Figure 23 and Figure 24 shows the measured waveforms of motor current and its speed without power factor corrector. The related motor speeds shown in Figure 23 and Figure 24 respectively.

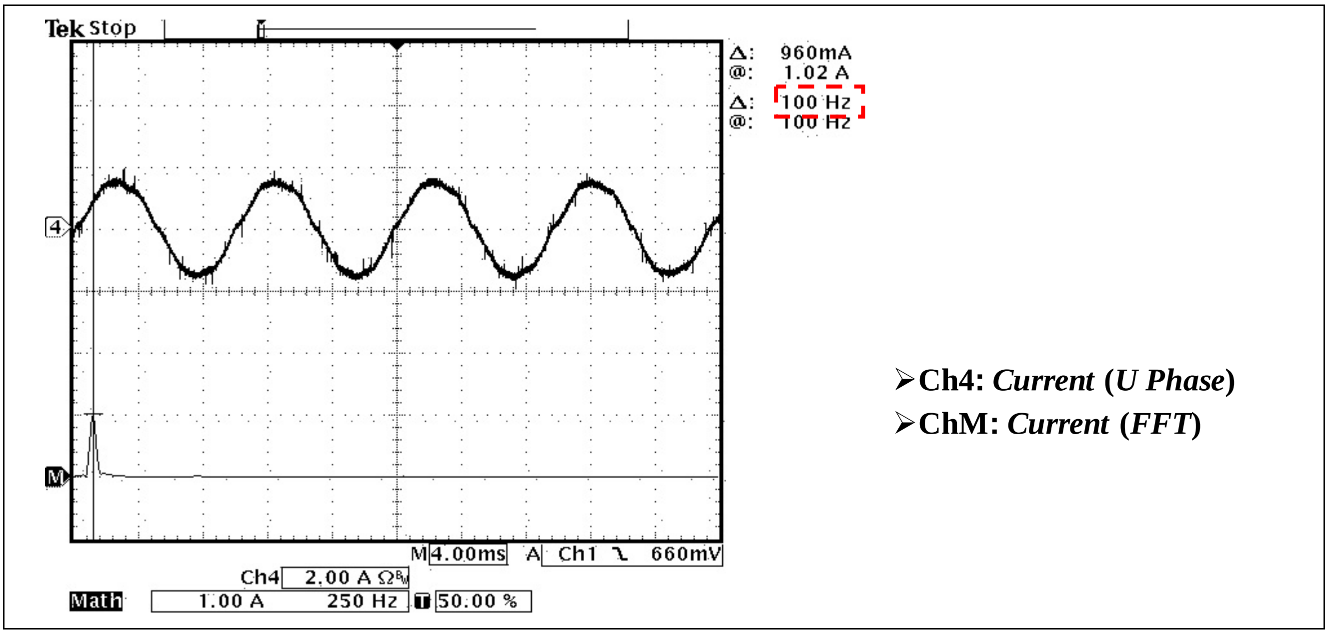

Figure 23 1500 rpm

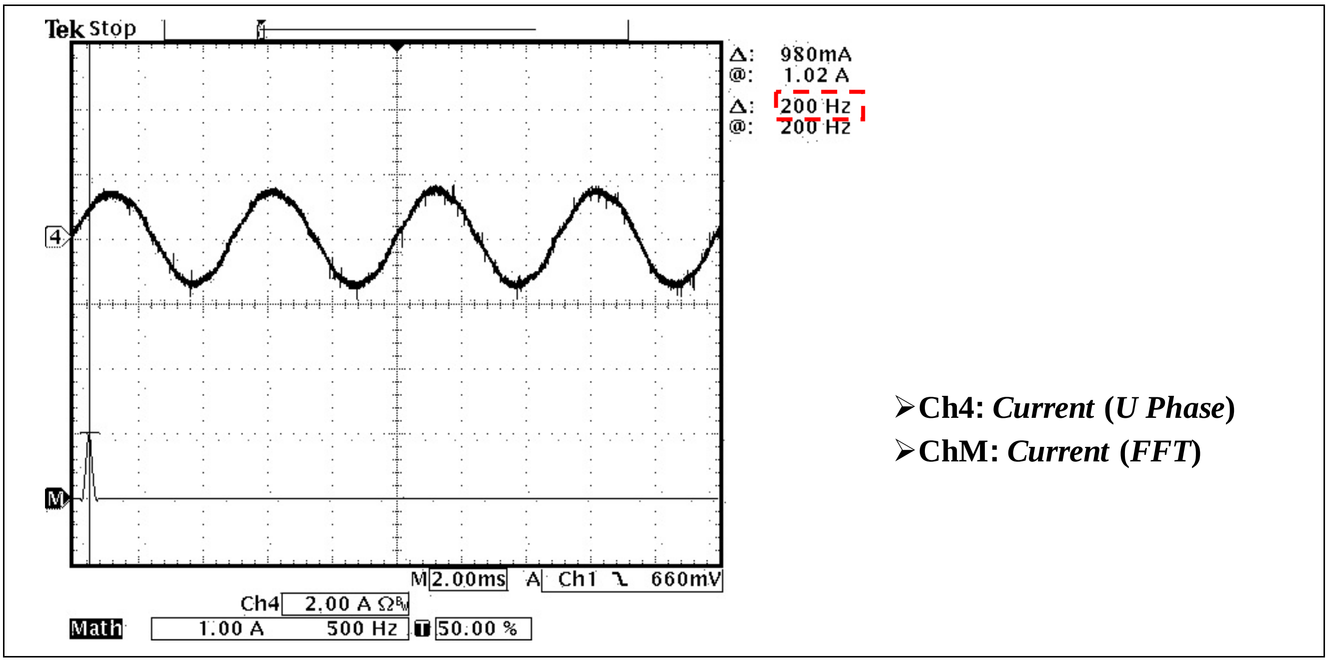

Figure 24 3000 rpm

Figure 25 shows the measured waveforms of motor control with power factor corrector. The related motor speeds shown in Figure 26 are 3000 rpm with power factor corrector.

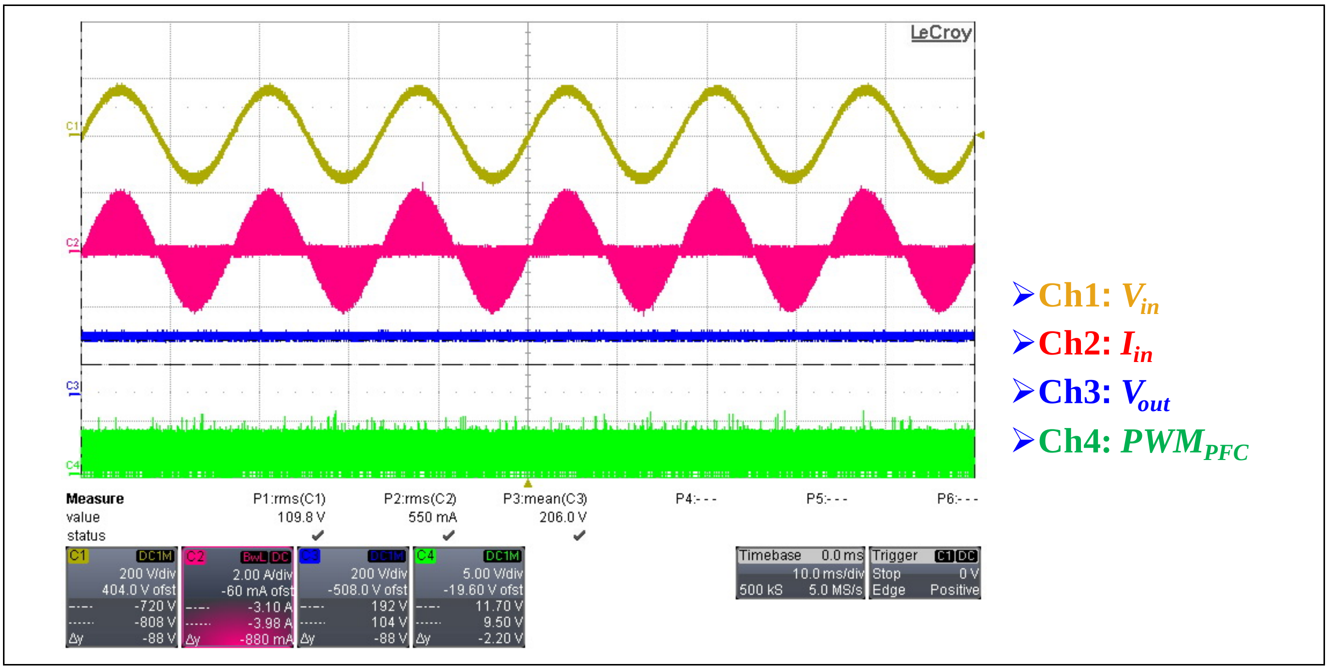

Figure 25 Measured waveforms of motor control with PFC

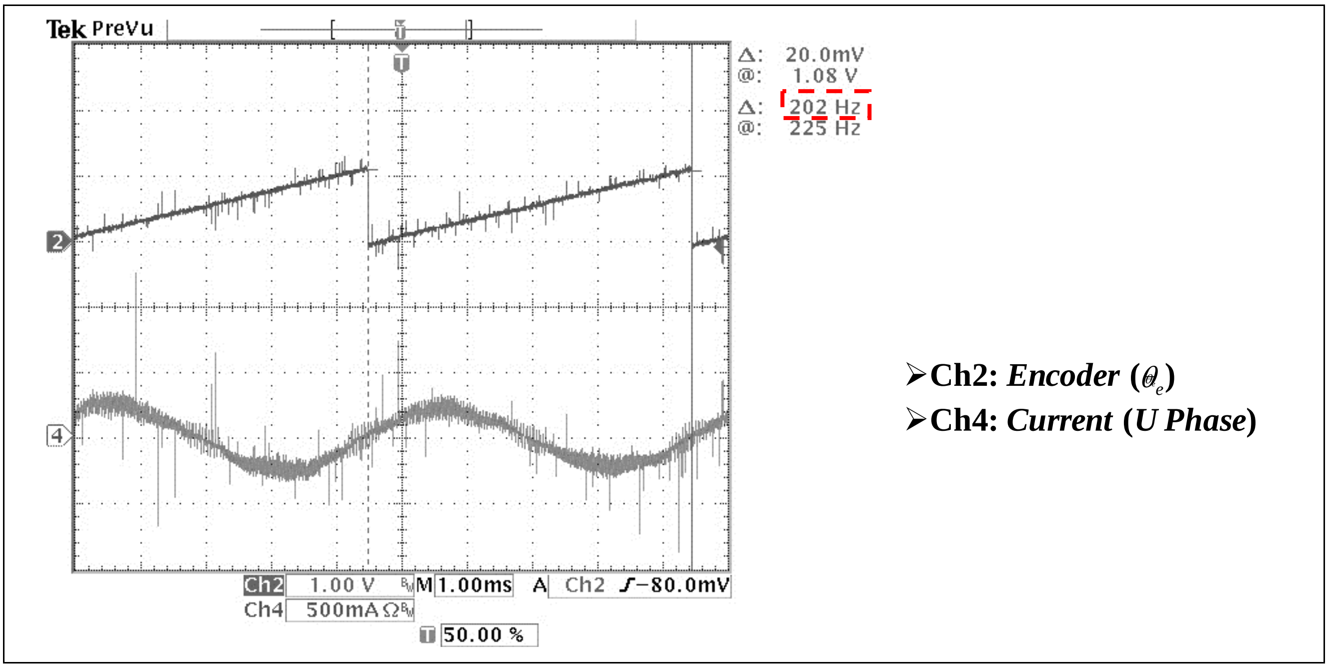

Figure 26 Relationship between encoder signal and U phase current

7. Conclusion

Power factor corrector and a vector-controlled PMSM drive are designed and implemented using RX210. Experimental results show the power factor goes up to 0.98 under full load condition and the motor speed goes up to its rated speed, 3000 rpm. These results demonstrate the results meeting the required specifications.

8. Reference

[1]. S. R. Bowes and Y. S. Lai, “The relationship between space vector modulation and Regular-sampled pulse-width modulation,” IEEE Trans. on Industrial Electronics, Vol. 44, No. 5, pp. 670-679, 1997.

Website and Support

Renesas Electronics Website
http://www.renesas.com/

Inquiries
http://www.renesas.com/contact/

Revision Record

Rev.	Date	Description	
		Page	Summary
1.00	Nov 01, 2012	—	First edition issued
1.01	Jan 23, 2013	—	Corrected only 3.3V power for VCC of RX210 on schematic file to fit the program using 3.3V

General Precautions in the Handling of MPU/MCU Products

The following usage notes are applicable to all MPU/MCU products from Renesas. For detailed usage notes on the products covered by this document, refer to the relevant sections of the document as well as any technical updates that have been issued for the products.

1. Handling of Unused Pins

   Handle unused pins in accord with the directions given under Handling of Unused Pins in the manual.

   — The input pins of CMOS products are generally in the high-impedance state. In operation with an unused pin in the open-circuit state, extra electromagnetic noise is induced in the vicinity of LSI, an associated shoot-through current flows internally, and malfunctions occur due to the false recognition of the pin state as an input signal become possible. Unused pins should be handled as described under Handling of Unused Pins in the manual.

2. Processing at Power-on

   The state of the product is undefined at the moment when power is supplied.

   — The states of internal circuits in the LSI are indeterminate and the states of register settings and pins are undefined at the moment when power is supplied.
   In a finished product where the reset signal is applied to the external reset pin, the states of pins are not guaranteed from the moment when power is supplied until the reset process is completed.
   In a similar way, the states of pins in a product that is reset by an on-chip power-on reset function are not guaranteed from the moment when power is supplied until the power reaches the level at which resetting has been specified.

3. Prohibition of Access to Reserved Addresses

   Access to reserved addresses is prohibited.

   — The reserved addresses are provided for the possible future expansion of functions. Do not access these addresses; the correct operation of LSI is not guaranteed if they are accessed.

4. Clock Signals

   After applying a reset, only release the reset line after the operating clock signal has become stable. When switching the clock signal during program execution, wait until the target clock signal has stabilized.

   — When the clock signal is generated with an external resonator (or from an external oscillator) during a reset, ensure that the reset line is only released after full stabilization of the clock signal. Moreover, when switching to a clock signal produced with an external resonator (or by an external oscillator) while program execution is in progress, wait until the target clock signal is stable.

5. Differences between Products

   Before changing from one product to another, i.e. to a product with a different part number, confirm that the change will not lead to problems.

   — The characteristics of an MPU or MCU in the same group but having a different part number may differ in terms of the internal memory capacity, layout pattern, and other factors, which can affect the ranges of electrical characteristics, such as characteristic values, operating margins, immunity to noise, and amount of radiated noise. When changing to a product with a different part number, implement a system-evaluation test for the given product.

SALES OFFICES Renesas Electronics Corporation http://www.renesas.com

Refer to "http://www.renesas.com/" for the latest and detailed information.

Renesas Electronics America Inc.
2880 Scott Boulevard Santa Clara, CA 95050-2554, U.S.A.
Tel: +1-408-588-6000, Fax: +1-408-588-6130

Renesas Electronics Canada Limited
1101 Nicholson Road, Newmarket, Ontario L3Y 9C3, Canada
Tel: +1-905-898-5441, Fax: +1-905-898-3220

Renesas Electronics Europe Limited
Dukes Meadow, Millboard Road, Bourne End, Buckinghamshire, SL8 5FH, U.K
Tel: +44-1628-651-700, Fax: +44-1628-651-804

Renesas Electronics Europe GmbH
Arcadiastrasse 10, 40472 Düsseldorf, Germany
Tel: +49-211-65030, Fax: +49-211-6503-1327

Renesas Electronics (China) Co., Ltd.
7th Floor, Quantum Plaza, No.27 ZhiChunLu Haidian District, Beijing 100083, P.R.China
Tel: +86-10-8235-1155, Fax: +86-10-8235-7679

Renesas Electronics (Shanghai) Co., Ltd.
Unit 204, 205, AZIA Center, No.1233 Lujiazui Ring Rd., Pudong District, Shanghai 200120, China
Tel: +86-21-5877-1818, Fax: +86-21-6887-7858 / -7898

Renesas Electronics Hong Kong Limited
Unit 1601-1613, 16/F., Tower 2, Grand Century Place, 193 Prince Edward Road West, Mongkok, Kowloon, Hong Kong
Tel: +852-2886-9318, Fax: +852 2886-9022/9044

Renesas Electronics Taiwan Co., Ltd.
13F, No. 363, Fu Shing North Road, Taipei, Taiwan
Tel: +886-2-8175-9600, Fax: +886 2-8175-9670

Renesas Electronics Singapore Pte. Ltd.
80 Bendemeer Road, Unit #06-02 Hyflux Innovation Centre Singapore 339949
Tel: +65-6213-0200, Fax: +65-6213-0300

Renesas Electronics Malaysia Sdn.Bhd.
Unit 906, Block B, Menara Amcorp, Amcorp Trade Centre, No. 18, Jln Persiaran Barat, 46050 Petaling Jaya, Selangor Darul Ehsan, Malaysia
Tel: +60-3-7955-9390, Fax: +60-3-7955-9510

Renesas Electronics Korea Co., Ltd.
11F., Samik Lavied' or Bldg., 720-2 Yeoksam-Dong, Kangnam-Ku, Seoul 135-080, Korea
Tel: +82-2-558-3737, Fax: +82-2-558-5141